SUMMARY OF USSR REPORTS ON MECHANICAL AND RADIOACTIVITY EFFECTS OF UNDERGROUND NUCLEAR EXPLOSIONS

Paul Kruger
Civil Engineering Department
Stanford University
Stanford, California

Two reports have been issued by the USSR which examine the mechanical effects and radioactive contamination of the environment from underground nuclear explosions (1,2).

In reviewing the mechanical effects, the Institute of Terrestrial Physics of the USSR Academy of Sciences (1) emphasizes the advantages of nuclear explosives, namely the tremendous power and small dimensions, in the industrial and construction fields. The authors note that the mechanical effects are based not only upon the explosive yield but also upon the thermodynamic properties of the cavity gases during expansion. These properties may vary widely depending upon the rock material.

A list of the basic parameters affecting the mechanical effects of contained nuclear explosions includes: cavity volume, dimensions of the chimney, degree of rock fracturing, intensity of the compression wave as a function of distance from shot point, and seismic effects.

From investigations conducted during the past few years in the Institute of Terrestrial Physics, the authors are able to relate the maximum dimensions of the cavity to the strength and elasticity of the rock by the equation:

$$V = \frac{W}{\rho c^2} \; f\left(\frac{\sigma^*}{\rho c^2}\right) \qquad (1)$$

where V = maximum cavity volume
W = explosion yield
ρ = rock density
c = longitudinal wave velocity
σ^* = radial stress at the edge of the elastic zone

The authors suggest, in discussing the maximum cavity size of contained nuclear explosions, that instead of assuming that the cavity expansion ceases when the cavity gas pressure equals the lithostatic pressure, accumulated data indicate that the cavity, upon reaching its maximum size, undergoes a certain compression. For example, evaluations made at the Institute of Terrestrial Physics indicate that the maximum cavity volume in the Salmon and Gnome events exceeded the final volume by 2 and 1.5 times, respectively.

With respect to chimney formation, several parameters are given which make delineation of explosion-produced effects difficult, e.g., irreversible

deformation of rock blocks, heating of the medium, microfractures, elastic properties of the rock, and individual elongated cracks. These criteria for description of the effects have not yet been analyzed.

Evaluation is being made of the use of the compression wave history as a means of describing the extent of rock fractures since the latter can be measured reliably and since the fracture radius is much greater than the cavity radius. Measurements can be made of the maximum velocity of the medium displacement in the wave. It is assumed that the amplitude of the displacement velocity can be scaled for explosive yield and distance by the equation:

$$v_{max} = C\left(\frac{W^{1/3}}{R}\right)^{1.6} \qquad (2)$$

where v = displacement velocity, μ/sec
W = explosion yield, kt TNT
R = displacement, μ
C = constant for the medium,
e.g., C=7 for granite, C=10 for rock salt

The seismic effect of the explosion is described in phases of source, propagation, and structures response. The source term is distinguished between contained and excavation explosions; considered a spherical compression wave for the former, and complex for the latter, in which the force of gravity plays an important role. The propagation through heterogeneous media under conditions of natural stratification is expected to be considerably different from propagation through an ideal elastic body.

Structures response is described by criteria established in the late 1930's in the Soviet Union. Experimental data for small explosions indicated that the maximum amplitude of surface displacement is the critical parameter which determines the danger zone for seismic effect. For small explosions, the threshold for damage to low rise buildings was determined to be approximately 10 cm/sec. This criterium is considered insufficient for large nuclear explosions because of the increased duration of the seismic signal. Further experiments are suggested to achieve a greater reliability for predicting seismic effects.

The mechanical effects of excavation by chemical explosives are described by the empirical equation:

$$W = k\,L^3\,f\left(\frac{R}{L}\right) \qquad (3)$$

where W = weight of the charge
L = line of least resistance
R = apparent radius of the crater
k = coefficient, involving the properties of the rock and the efficiency of the explosives.

In comparing the effects of a nuclear explosion to the experiences gained with chemical explosives, it is noted that two characteristics are especially important, i.e., the greater initial energy density, making the thermodynamic properties of the rock more important, and the large scale of the explosions, making geometrical scaling laws unreliable. The gas acceleration phase of the nuclear explosion depends to a greater extent upon the presence of moisture and volatile products in the rock.

For excavation explosions, the list of basic parameters includes: dimensions of the crater, distribution of the ejecta, seismic effect, and foundation

and slope stability. The properties of the medium with depth are also important in large-scale explosions; e.g., rock strength, scale of inhomogeneities, and fracture distribution. With these parameters generally unknown and the above characteristics of nuclear explosions, it is doubted that the scaling laws for excavation effects are adequate. Research is strongly recommended on modeling explosions. A special facility for simulating explosions accompanied by ejection in loose soils has been designed at the Institute of Terrestrial Physics. Results on the dependence of the crater radius upon the explosion energy have been satisfactorily obtained.

The phenomenology of radioactive contamination of the environment was described by Izrael, et.al. (2) for both contained and excavation explosions. They consider as the major restraint upon peaceful uses of nuclear explosions the radiation from the nuclear debris which contaminates the natural environment or the industrial products either removed from or stored in the explosion-produced cavities. They also consider it possible to avoid or reduce the radioactivity hazards for industrial use and to arrive at reasonable criteria and standards for radioactive debris beyond national borders.

The radioactivity history is influenced markedly by the hydrodynamic phase of the explosion. For example, the authors consider the temperature changes in the cavity during expansion. They noted that for media with 6.5 or less percent volatile materials, the cavity temperature at maximum cavity size will remain above the condensation temperature of the media. In excavations, where the gas phase imparts additional acceleration to the surface layers, the water content of the rock is an important parameter.

The description of the venting from an excavation nuclear explosion is illustrated with the geonuclear effects of the USSR test "1003". The data for this explosion and the dimensions of the crater configuration are summarized in Table 1. External observations of the shot noted the gas acceleration phase at 0.25 sec when the dome had a height of about 7 m and was rising with a velocity of 60-70 m/sec. Venting occurred at 0.4 sec when the dome had a height of 19 m and a peak velocity of 170 m/sec. The temperature of the luminous area reached 1900-2100°C at about one second.

The base surge spread in 35-40 sec with a diameter of 600 m, and the main cloud, 120 m diameter, rose to a height of 300 m, restricted by the presence of a temperature inversion.

It was noted that for deeply-buried explosions, venting can occur only through fissures and cracks in the geologic media. Since the flow rate of gases through such media is a relatively slow process, only the rare gas nuclides, primarily the krypton and xenon fission products, or very volatile elements, e.g. the halogens, can escape to the atmosphere. An expression is given for the time-integrated release of a particular nuclide, A_i:

$$A_i = 1.45 \times 10^{23} M_i W \frac{\lambda_i k}{k + \lambda_i} e^{-\lambda_i t_o} \qquad (4)$$

where

M_i = cumulative fission product yield of isotope i

W = fission yield, kt

λ_i = decay constant of isotope i

k = release rate from the cavity, the fractional volume removed per unit time

t_o = time since venting

Since the cavity gas temperature remains above the condensation temperature for a time long compared to the half lives of the rare gases, fractionation of fission products inside the cavity is not great. However, the initial distribution of the longer-lived daughter radionuclides, such as Sr^{89}, Sr^{90}, and Cs^{137}, having gaseous precusors depends upon the fracture and venting history. Fractionation of such nuclides can be great.

For scaled depths of burial less than 60-90 $m/kt^{1/3.4}$, venting and break through of the cavity gases is expected, accompanied by the formation of a base surge and a main cloud. The zones of radioactive contamination that must be considered include the base surge and main cloud in the atmosphere, the fallback and ejecta at the crater site, and the local and distant fallout tracks. The extent of the contamination of each of these zones is influenced by the total production of radioactivity, the vent fraction, and the degree of dilution in the atmosphere resulting frrm the prevailing meteorological conditions. The total amount of radioactivity includes both the fission products and the neutron-induced radioactivity.

The intensity (I, in Mev/sec) from the γ-ray emitting radionuclides produced in a 1 kt fission explosion as a function of time (t, in days) is shown as curve 1 in Figure 1. For industrial nuclear explosions in which the fission yield is a small part of the total explosive yield, the induced radioactivity plays an important role. Curve 2 in Figure 1 shows the corresponding data for the induced activity for equal integrated doses. The calculations of induced activity was based on thermal neutron irradiation of media with the chemical composition of clarkeite. For neutrons in the energy range of 10-100 eV, calculations show similar results for $t \leq 3.0$ days. The dashed curve in Figure 1 shows the greater induced activity for the period $10 \leq t \leq 300$ days expected for the higher-energy neutron activation. For the first 5 days, Na^{24} is the principle γ-ray emitting radionuclide. From 1 month to 1.5 years, Sc^{46} and Fe^{59} add significantly to the fission product gamma radiation; after 1 year, Co^{60} is important; and after 10 years, Eu^{152}.

The ratio of doses from induced activity, D_n, to fission product activity, D_o, can be estimated for contained nuclear explosions in which no significant fractionation occurs, from the ratios of the respective gamma radiation energies by

$$\frac{D_n}{D_o} = \frac{E_n}{E_o} = \frac{1.4 \times 10^{22}\ t_b^{0.2}}{W}\ \Pi \Sigma_i\ \alpha_i\ E_{\gamma_i}\ e^{-\lambda_i t_b} \qquad (5)$$

where

W = fission yield, g fissioned material

Π = total neutron flux

α_i = the fraction of neutron producing the i^{th} isotope

E_{γ_i} = the γ-ray energy of isotope i

λ_i = the decay constant of isotope i

t_b = fallout time period along the track

For close-in fallout, where $t_b \cong 2$-3 hours, the main dose from Na^{24} radiation, with $E_\gamma = 4.14$ Mev, leads to

$$\frac{D_n}{D_o} \cong 1.2 \times 10^{-23}\ \frac{\alpha\, \Pi}{q_g} \qquad (6)$$

For $\alpha = \alpha_{Na} = 0.09$, and $\Pi = 10^{24}$ neutrons, the two doses become equal for a yield, $W = 1$ kt or $q_g \cong 60$ g.

The two dose contributions can be combined into an "effective" fission yield without contribution from neutron activation which gives the same dose by

$$q_{eff} \cong q_g + 2.5 \times 10^{-24} t_b^{0.2} \Pi \sum_i \alpha_i E_{\gamma_i} e^{-\gamma_i t_b} \quad (7)$$

This simplifies, for the close-in fallout track, to

$$q_{eff} \cong q_g + 10^{-24} \Pi \quad (8)$$

The vent fraction is described as a function of yield and depth of burial by the scaled depth of burial parameter,

$$\bar{h} = \frac{h}{W^{1/3.4}} \text{ or } \frac{h}{W^{1/3}} \quad (9)$$

Figure 2 shows the vent fraction, $\varphi(\bar{h})$, calculated for the USSR "1003" test and for 4 USA events. The vent fraction is also noted to be influenced in many cases by the properties and texture of the media and its water content. The authors note that the fraction of radioactive debris which remains in the radioactive cloud beyond the fallout track is only about 1 percent of the total radioactivity production and is likely to be constant for explosions within the range of scaled depths of burial of 35-55 $m/kt^{1/3.4}$.

The height of radioactive cloud (800m) for the Soviet "1003" experiment is compared to the USA Sedan (4200m) and Danny Boy (no main cloud) experiments. The characteristics of the"1003" cloud were determined by geophysical rocket probe sampling and by aircraft. The maximum radiation level in the cloud 107 minutes after the explosion was 0.82 r/hr. The cloud contained about 1.2 percent of the γ-ray emitting products of the explosion. Table 2 shows the ratio of dose from cloud radiation, D_c to radiation dose from deposited radioactivity, D_f as a function of distance from ground zero (G.Z.) in km.

Physical and chemical descriptions of the radioactive particles in the cloud are given. The particle shapes were generally irregular and of varying structure, including slag-like porous particles and "sugar-like" particles. The particle size distribution for samples collected between 0.3 to 4 hours generally followed a log normal distribution. About 90% of the radioactive particles had a diameter less than 0.5μ; the median diameter was about 2μ. The radioactivity content of the particles at 3 seconds was about 80% for particles with diameter greater than 10μ, while particles with diameter less than 0.5μ contained only 1%. Solubility tests with water and with 20% HCl a week after the explosion showed that 70 to 90% of the total activity of the sample was soluble. Nuclides such as I^{131}, Te^{132}, Ru^{103}, and Ce^{141} were about 70-80% soluble, while Ba^{140} was 90%.

The isotopic composition of debris in the base surge and the cloud were determined after sampling by rockets and aircraft and with radiochemical separations and γ-ray spectroscopy radiation measurements. Table 3 lists the enrichment factors of several fission products, relative to the number of Zr^{95} nuclei, for several characteristic samples. The data indicate that the dust column becomes impoverished with respect to volatile nuclides as well as those with volatile precusors after a few seconds. Cloud samples taken 70-80 km from G.Z. are enriched in these nuclides. The nuclides identified include Sr^{89}, Sr^{90} + Y^{90}, Sr^{91} + Y^{91}, Cs^{137}, Ba^{140} and smaller amounts of Ru^{103} and Ce^{141}. The isotopic composition of the dust column is similar to those of the fallback and ejecta samples.

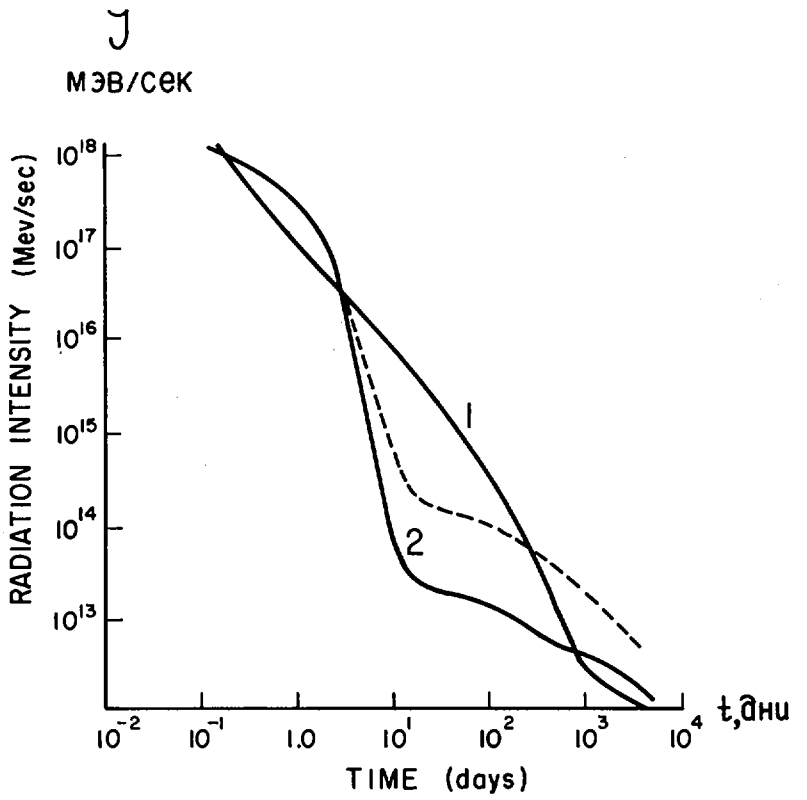

Figure 1. The γ-ray intensity of radionuclides from a 1 kt fission explosion as a function of time.

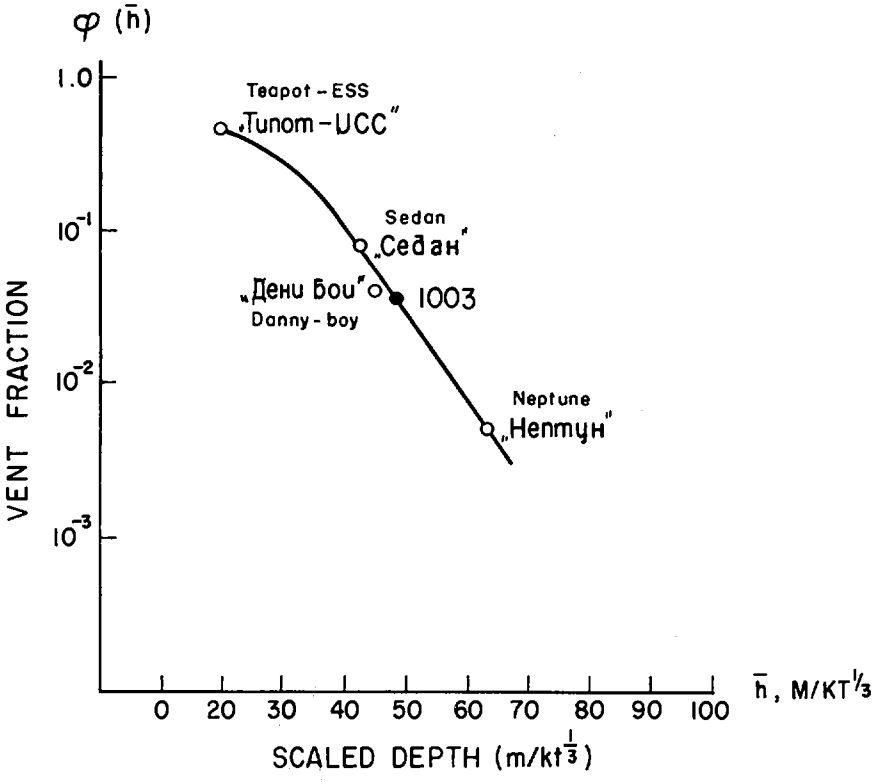

Figure 2. The vent fraction as a function of scaled depth of burial

TABLE 1

THE USSR "1003" NUCLEAR EXCAVATION

EXPLOSION DATA:

W = 1 KT ; All Fission

Z = 48 meters

Medium: Jointed Sandstone

ρ = 2.57-2.80 g/cm^3

Moisture = 0.8 wt %

RESULTS:

D_a = 31 m

R_a = 55 m

R_{al} = 65 m

R_{eb} = 150m

TABLE 2

RATIO OF CLOUD TO FALLOUT DOSES ALONG FALLOUT TRACK

	DISTANCE FROM GROUND ZERO (KM)				
	8	11	25	44	49
$\frac{D_c}{D_f}$	0.5	1.2	5.7	13.8	23.5

TABLE 3

ISOTOPIC COMPOSITION OF "1003" DEBRIS

Post-Explosion Sampling Time	Location	Zr^{95}	Zr^{97}	Ce^{144}	Mo^{99}	Ce^{141}	Ru^{103}	Ru^{106}	I^{131}	Ba^{140}	Y^{91}	Cs^{137}	Sr^{89}
3 sec	Dust Column above G.Z.	1.0	-	0.89	1.12	1.07	0.8	1.16	0.96	0.79	0.57	0.25	0.001
5 sec	Dust Column above G.Z.	1.0	1.12	0.75	1.12	0.63	1.28	0.0019	0.0094	0.37	0.31	0.1	0.0043
1.5 hrs	Main Cloud R = 70 km	1.0	1.08	0.89	1.1	4.9	3.35	0.63	0.175	37.4	26.2	34.8	93
2.4 hrs	Main Cloud R = 80 km	1.0	0.99	0.76	1.1	5.3	5.4	0.9	1.2	24.6	18.2	19	47.7
-	Crater Rubble	1.0	-	0.9	1.26	0.72	0.16	0.10	0.21	0.42	0.40	-	0.048
-	Lip Ejecta	1.0	-	0.94	-	1.6	0.34	0.51	0.42	0.83	0.95	0.226	0.176

An analysis is reported on the fractionation of radionuclides in the main cloud for nuclear excavations which had substantially different filtering properties during the mound disassembly. The "normal" excavations, "1003" and Danny-Boy are compared in Table 4 to Sulky, which created a rubble mound, and to Palanquin, which created a crater by gas-venting erosion.

The fallout pattern of the "1003" event was investigated for the distribution and time behavior of radiation levels, the partition of radioactivity between the off-site and on-site zones, and the depth profile of radioactivity in the ejecta zone. From aerial gammagraphs and with radiochemical analysis, γ-ray energy intensities were contoured at an elevation of one meter. The radiation levels in the fallout pattern were determined by integrating the radiation levels along the track's axis and transverse to its axis:

$$Q_{s\ell} = \int_R \int_\ell p(R,\ell)\ dR\ d\ell \qquad (10)$$

where

$Q_{s\ell}$ = radiation level in the fallout pattern, (r/h) (km^2)

$p(R,\ell)$ = radiation intensity at (R,ℓ), at an altitude of 1 m, r/hr

R = distance along the track axis, km

ℓ = distance along the transverse axis, km.

This method differs somewhat from the U. S. method of integrating within the limits of the isolines. The total fallout was calculated on the basis that a radiation intensity of 1 (r/hr) (km^2) corresponds to the energy release of 2.86 x 10^{15} Mev/sec. The deposition fraction is scaled to the total production of radiation produced in a 1 kt explosion.

Figure 3 shows the iso-intensity contours around the crater area, Figure 4 shows the fallout pattern along the cloud track, and Figures 5 and 6 show the distribution of radiation intensity at several times along the track's axis and along the transverse axis, respectively. It was noted that the mean velocity of the main cloud was about 40 km/hr, corresponding to the average wind speed in the 0-0.5 km layer. The radiation intensity was measured out to about 300 km, where, at H + 24 hours, the value at the surface was 5 μr/hr. The fraction of radioactivity deposited in the off-site fallout pattern was estimated to be 3.5% of the total amount produced. A comparison of the cloud velocity and fallout fraction for "1003" and several US excavation tests is given in Table 5. A comparison of the relative radiation intensities at H + 24 hours along the track's axis is shown in Figure 7. The curves are all adequately described by the inverse-square law. It is noted that the relative intensity is not affected significantly by the geometry of the source and the distribution of the radionuclides.

The depth profile of the lip was determined by radiochemical analysis of soil layers. Figure 8 illustrates the relation of activity with depth. The decrease is described by the empirical equation

$$A(z) = A_o\ e^{-0.066\ z} \qquad (11)$$

where

A_o = surface layer activity

z = depth, cm

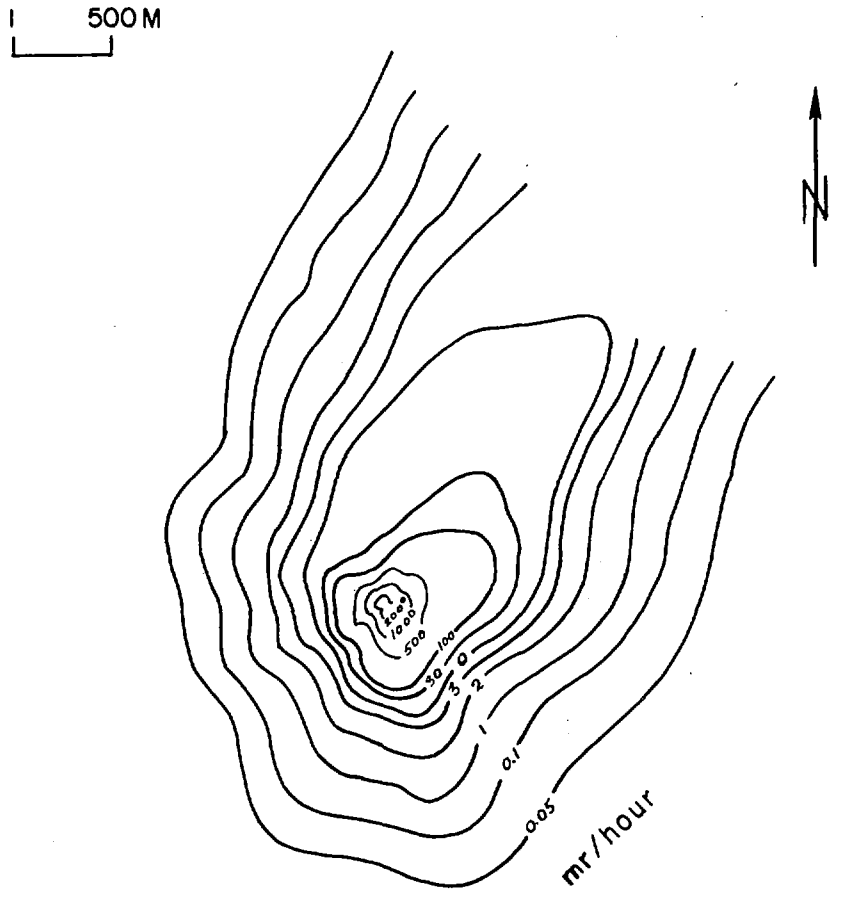

Figure 3. Gamma-ray intensity contours around the USSR "1003" nuclear excavation

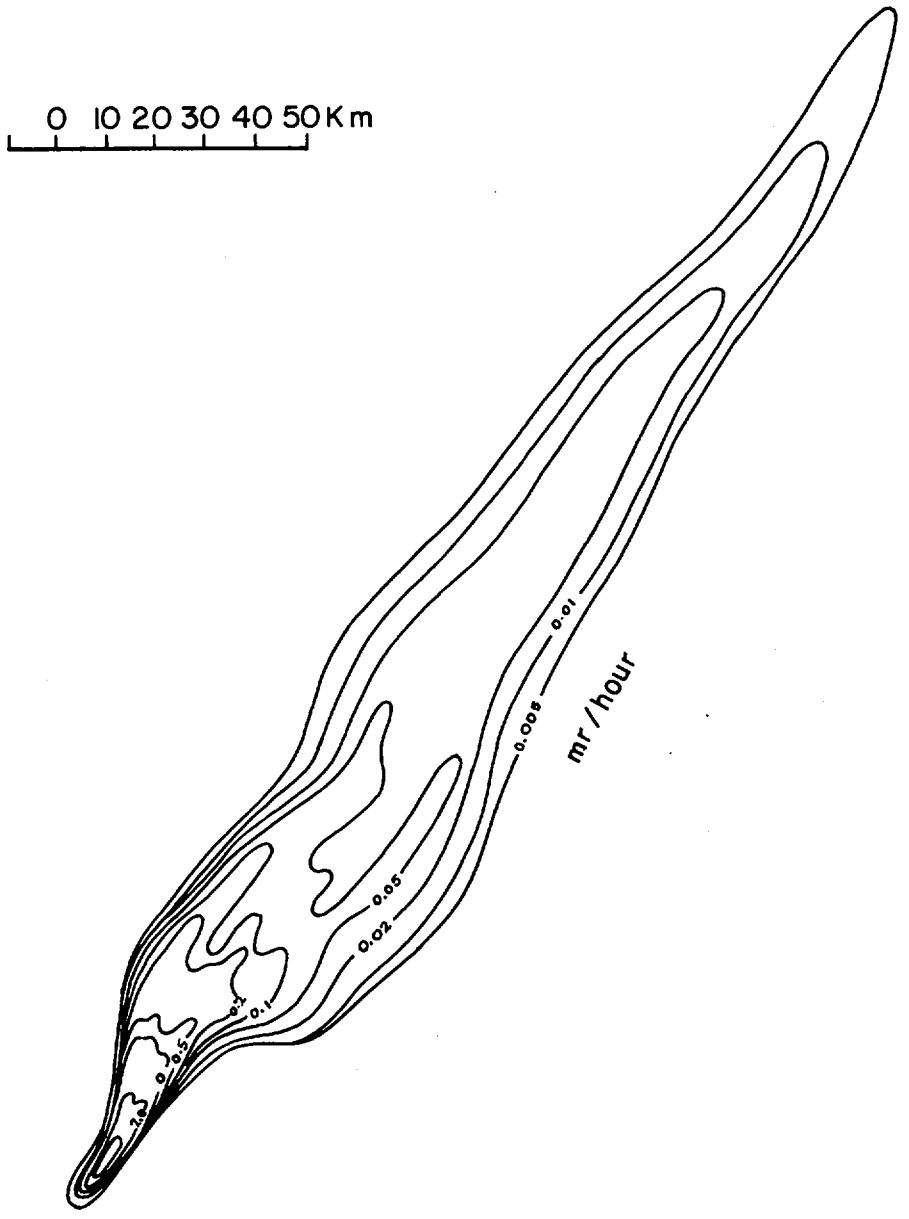

Figure 4. Fallout pattern along the "1003" cloud track.

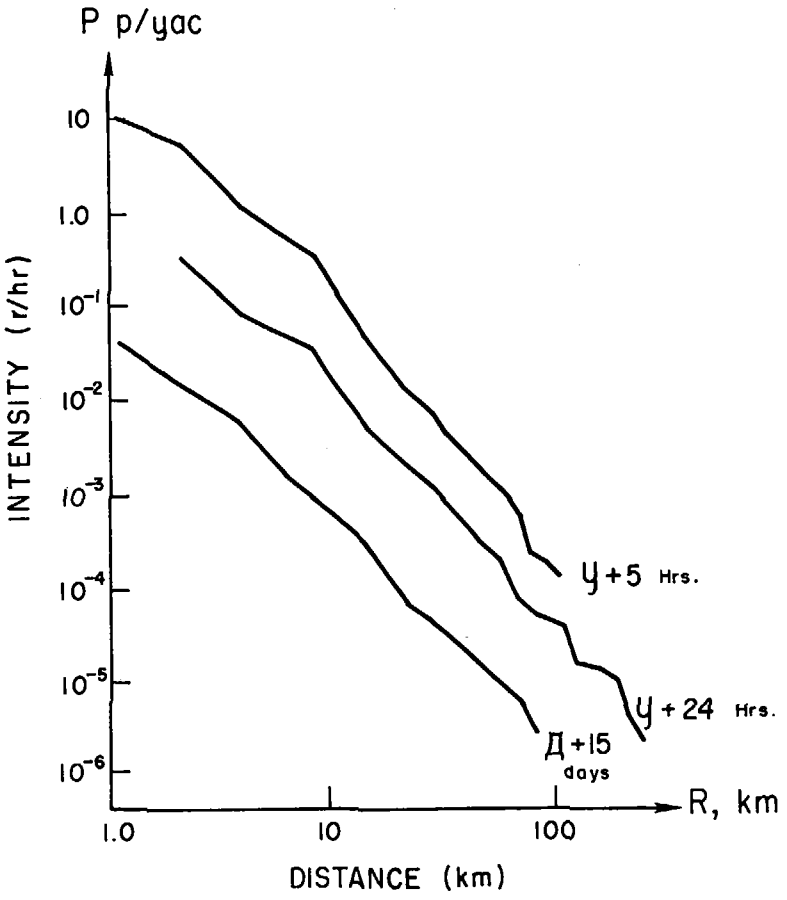

Figure 5. Radiation intensity along the "1003" track axis.

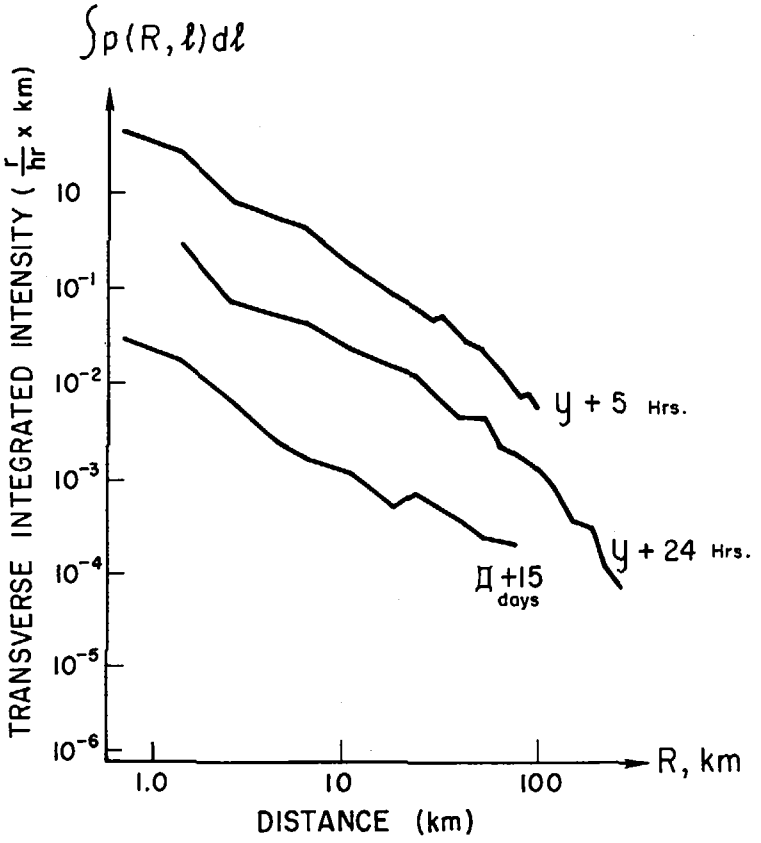

Figure 6. Radiation intensity along the "1003" transverse axis.

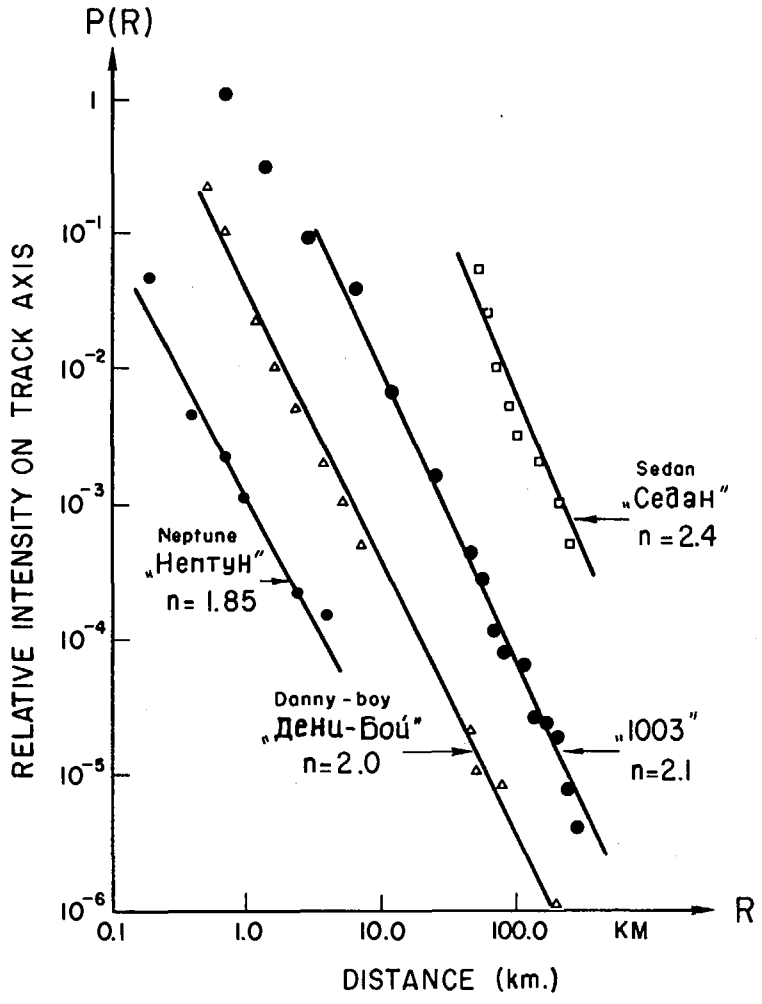

Figure 7. Comparison of radiation intensity along the track axis for several nuclear excavations.

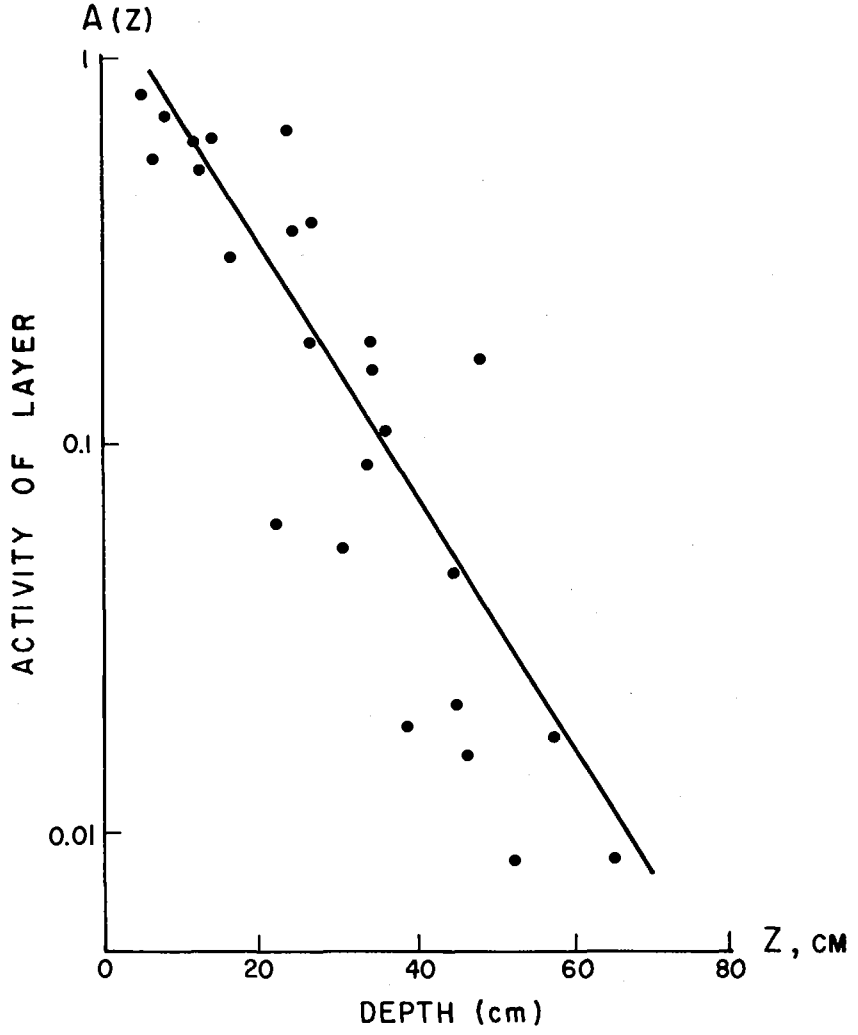

Figure 8. Radioactivity profile with depth in the "1003" crater lip.

It is noted that the activity at 1 meter was 1/100 of the surface activity and that 90% of the radioactivity is contained in the upper 52 cm. The total activity of the ejecta material was 10-15% produced. The isotopic composition is shown in Table 6. The depletion of the nuclides with gaseous precursers is also noted.

The volatile fission products in the cloud were followed by aircraft sampling using $AgNO_3$ and activated charcoal filters. The nuclides Xe^{133} and Xe^{135} were found, essentially unfractionated, during the period of 4 to 98 hours. Iodine isotopes were also detected, but the levels were reduced by factors of 10^3 to 10^4. The maximum radiation level of 2 mr/hr at 15 km from G.Z. occurred at H + 4 hours at an altitude of about 50 m. The flow rate of the radioactive gases at H + 74 hours was 1260 Ci/hr. The aerosol particles in the cloud were examined for their particle size distribution and their solubility.

The isotopic composition of the particles deposited on pans and soil out to 50 km were determined by radiochemical methods. The general observations included (1) deficiency in nuclides with gaseous precurors, (2) same composition as the ejecta, but with a slight enrichment of the volatile-precursor nuclides on the windward side of the crater, and (3) a decrease in apparent fractionation with distance along the track axis. The extent of isotopic fractionation was calculated in the same manner as for U. S. Tests. The isotopic fractionation coefficients for several nuclides are listed in Table 7.

The activity induced in the "1003" media is compared to that from a low-power USSR underground nuclear explosion in a salt bed. The production of radionuclides (relative to Zr^{95}) in samples from these two explosions is shown in Table 8. The difference in activation between salt and silicate rocks is readily apparent. At D + 200 days, the major activation products from "1003" were Mn^{54} (65%) and $Eu^{152,154}$ (23%), while those from "Camouflet" were Sb^{124} (90%) and Ta^{182} (8%).

The solubility of the fallout radioactivity was measured to estimate the hydrologic transport by overland flow, contamination of open reservoirs, infiltration into ground water, migration in soils, and biological availability. Leaching of the base surge and cloud fallout with distilled water indicated the solubility of the same nuclides as those on crater fallback and ejecta which are soluble. The relative content of the leach water was: Sr^{89} ~ 70-90%, Sr^{90} ~ 4-6%, Ba^{140} ~ 0.5-2%, $Ru^{103,106}$ ~ 7-20%, and Sb^{124} ~ 1.4-7%. The solubility coefficients of some of these nuclides, along the track axis, are illustrated in Figure 9.

The solubility data of these nuclides are related to their gaseous-precursor history; the most soluble nuclides being those adsorbed on particle surfaces after formation from their gaseous precursors. The solubility of nuclides without gaseous precusors was very low. The solubility coefficients are ordered, relative to 1.0 for Sr^{90}, as follows:

Sr^{89}	>	Sr^{90}	>	Sb^{125}	>	Ba^{140}	>	$Ru^{103,106}$	>	Cs^{137}	>	Cs^{134}	>	(Mn^{54} Co^{60} Ce^{144} Y^{91} Zr^{95})
1.25		1.0		0.3		0.24		0.01		0.04		0.02		0.01-0.001

The redistribution or subsequent transport of the radioactive debris has been examined for hydrologic transport, wind redistribution, and foliar deposition. During the year following the"1003" detonation, ground water flowed into the crater to a total volume of about 100 m^3. Radiochemical studies of the water in the crater were undertaken to examine the way the crater filled and the role played by groundwater in creating artificial reservoirs. The major nuclides observed were Sr^{89}, Sr^{90}, Ru^{103} and Ru^{106}. Also detected were Sb^{125} and Cs^{137}. From the data in Table 9, it was noted that the solubility properties were in agreement with expectations according to the position of the

TABLE 4

ISOTOPIC ENRICHMENT FACTORS IN THE "1003" MAIN CLOUD
(RELATIVE TO ZR-95)

NUCLIDE	PALANQUIN	DANNY-BOY	"1003"	SULKY
Sr^{89}, Cs^{137}	1-2	15-100	20-98	10^5
Ba^{140}	1.0	10	25-37	1.5×10^4
Ce^{141}	1.0	3.0	5.0	12

TABLE 5

COMPARISON OF USSR "1003" TO USA EXCAVATIONS

Event	W (kt)	h (m)	$\bar{h}$ ($m/kt^{1/3.4}$)	$\bar{h}$ ($m/kt^{1/3}$)	Dia. (m)	H (km)	V (km/hr)	Fraction of Radioactivity in Fallout (%)
"1003"	1.0	43	48	48	130	0.3	40	3.5
Sedan	100	194	50	42	370	4.5	22	~8.0
Danny Boy	0.42	33.5	43	45	65	0.3	24	4-7
Neptune	0.115	30.5		63	60	1.2	25	0.5
Teapot Ess	1.2	20.4		19	89	2.4		46

TABLE 6

ISOTOPIC COMPOSITION OF SURFACE EJECTA

Nuclide	Fraction (%)
Zr^{95}	14
Ru^{106}	14.2
Ru^{103}	13.6
Ce^{141}	15.1
Ce^{144}	15.0
Ba^{140}	11
Sr^{89}	6.0
Sr^{90}	9.4

TABLE 7

ISOTOPE FRACTIONATION COEFFICIENTS

Isotope	$(f_{i,95})_{ave}$	Range of Values
Sr^{89}	0.38	0.18-0.80
Sr^{90}	0.45	0.19-0.87
Ba^{140}	0.80	0.55-1.28
Ce^{141}	0.90	0.69-1.96
Ru^{103}	1.15	0.87-1.55

TABLE 8

RELATIVE PRODUCTION OF ACTIVATION PRODUCTS

Event	Sample	$N(Zr^{95})$ (10^9 atoms/g)	RATIO OF N(i) TO $N(Zr^{95})$								
			Co^{60}	Mn^{54}	Zn^{65}	Ag^{110m}	Sb^{124}	Cs^{134}	Eu^{152}	Eu^{154}	Ta^{182}
"1003"	Ejecta	129	0.07	7×10^{-4}	-	-	-	0.01	-	-	-
"1003"	Ejecta	167	0.06	6×10^{-4}	-	-	-	0.01	-	-	-
"1003"	Crater Rubble	3408	0.13	0.01	0.001	-	-	0.02	0.03	0.02	0.004
Camouflet	Salt	233	0.06	0.06	-	0.08	0.97	-	Tr	Tr	0.16

TABLE 9

SOLUBILITY DISTRIBUTION IN USSR UNDERGROUND EXPLOSIONS

NUCLIDE	IN WATER IN A NUCLEAR CRATER (% in)			IN WATER FROM A CAVITY IN SALT (% in)		
	Colloids	Cations	Anions	Colloids	Cations	Anions
Sr^{90}	none	100	none	none	100	none
Cs^{137}	1.5	98.5	none	1.2	98.2	none
Ru^{106}	19.4	5.1	75.5	25.7	11.6	62.7
Sb^{125}	6.5	8.5	85	none	6.2	93.8

elements in the periodic table. The changes in concentration with time are illustrated in Figure 10.

Groundwater transport of the radionuclides was studied with a network of observation wells established at the "1003" site, at depths of 26 to 50 m, and located from 200 to 700 m from the emplacement hole. Systematic hydrogeological observations were begun two months after the detonation. The authors noted that the crater shape was preserved during the one year period and that the water levels in the wells were lowered by 0.7 to 1.3 m. They concluded that infiltration of groundwater into the crater occurred. Measurements in the observation wells confirmed the absence of radioactivity contamination in the wells even after several years following the explosion.

A series of laboratory measurements were made on the solubility of radionuclides on fallback and ejecta materials. Various solutions were used, such as distilled water at several pH, water with dissolved solids (Ca, Mg, Na, Cℓ) at a concentration of 1.3 g/ℓ, HCℓ solution, and water with EDTA complexing agent. The distribution coefficients for mass to volume ratios of 2 to 200 were determined for solution contact time of 10 days at room temperature. As an example, the results of the experiments with the water containing 1.3 g/ℓ of dissolved solids and crater rubble samples, conducted from D + 150 to D + 250 days, are shown in Figure 11. It was noted that for this time period, the soluble nuclides were $Sr^{89,90}$, $Ru^{103,106}$, and Sb^{125} with traces of $Ce^{141,144}$ and Zr^{95}. Effects for specific radionuclides were noted in the experiments with varying volume to mass ratios, particle size distributions, and pH. Little effect was noted for changes in dissolved solids concentrations form 0.13 to 13 g/ℓ.

Transport by secondary dust redistribution was examined for varying wind conditions and for on-site operations by heavy earth-moving equipment and motor vehicles. Experiments were carried out during one summer at three selected sites around the crater, at which the dose rate, thickness, moisture content, particle size distribution, and surface wind speed were examined. Air contamination was noted to be influenced markedly by the moisture content and wind velocity. For example, at constant wind velocity, the concentration of radioactive material in the air increased by about a factor of 10 when the ground moisture decreased from 10.6 to 3%. For constant ground moisture of 3%, the concentration increased a factor of 5 when the wind velocity changed from 0.6 m/sec to 5 m/sec. Air contamination caused by motor vehicles was noted to be ten times, or more, greater than in the case of natural dust formation. The concentrations ranged from 0.5 to 500 x 10^{-12} Ci/ℓ. Foliar deposition was noted to be influenced by the extent of secondary wind redistribution. Differences in radionuclide composition of the foliar deposition and those at root level were noted.

A model for fallout prediction has been developed. The basic parameter in estimating the fallout pattern in the absence of wind shifts in the atmosphere is the settling velocity, v, of the radioactive particles. A simplification of the radioactive particle distribution in the base surge and main cloud is assumed such that at altitude H there is a point source of a polydispersed aerosol with distribution N(v), for which the observed fallout pattern can be calculated. The expression for the fallout pattern resulting from this distribution with a wind velocity V is

$$p(x,y) = \frac{QHV\ N(\frac{HV}{x})}{\sqrt{2\pi}\ \sigma_y(x)\ x^2}\ e^{-\frac{y^2}{2\sigma_y^2(x)}} \qquad (12)$$

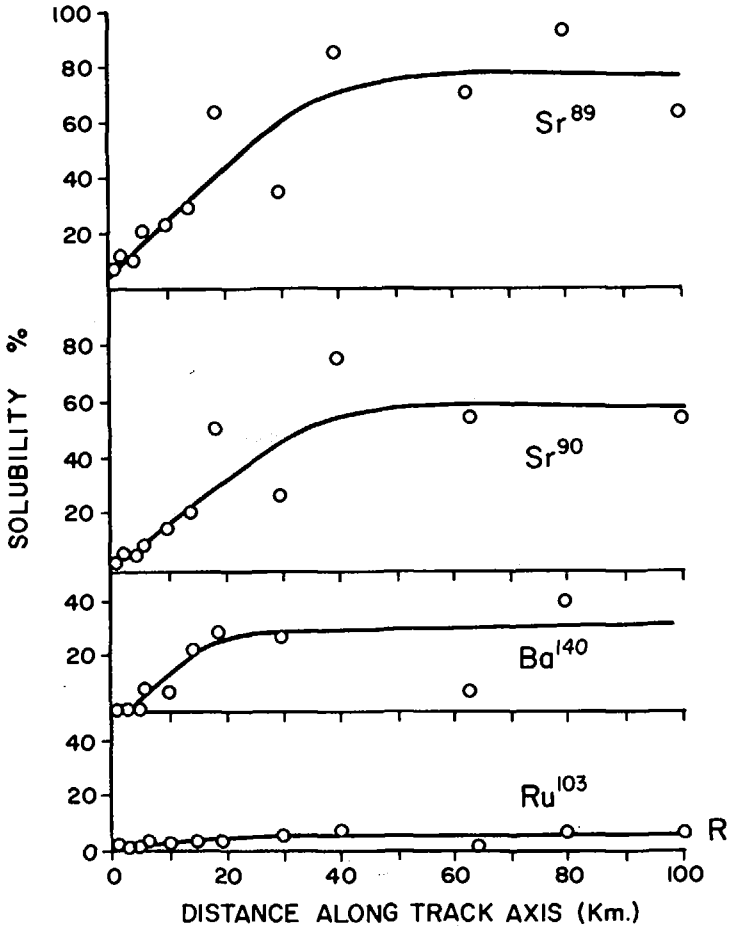

Figure 9. Solubility of radionuclides deposited along the track axis.

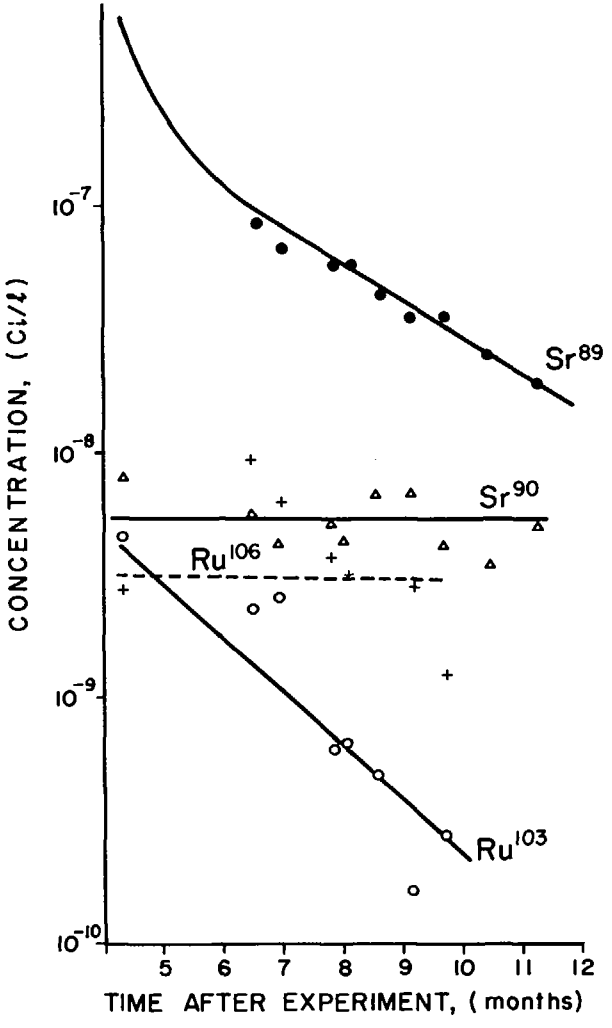

Figure 10. Radionuclide concentrations in crater water as a function of time.

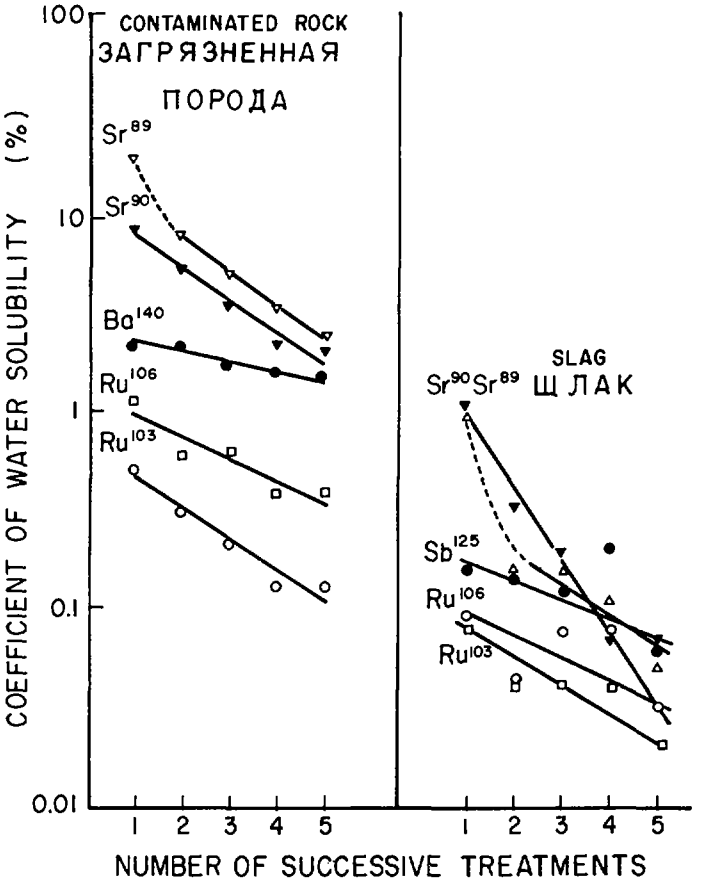

Figure 11. Radionuclide solubility as a function of successive exposures to water.

where

Q = total source strength, Ci

$\sigma_y^2(x)$ = the dispersion of the distribution $p(x,y)$ in the y direction, km

$N(\frac{HV}{x})$ = volume density of particles according to particle settling velocity, $v = \frac{HV}{x}$

The total radioactivity at $t = h + 1$ hours is related to the explosive yield W (in kt) by $A(h + 1) = 4.5 \times 10^8 W$ and the dose rate can be related to the fallout pattern by

$$D(h = 1\ m) = k_1\ p(x,y)$$

where $k_1 \cong 10^{-5}$ r/hr/Ci/km^2.

Thus, equation (12) may be rewritten

$$p_t(x,y) = \frac{CWI(\bar{h})HVF(v)}{\sqrt{2\pi}\ \sigma_y(x)x^2}\ e^{-\frac{y^2}{2\sigma_y^2(x)}} \tag{13}$$

where

$p_t(x,y)$ = γ-ray dose rate from the fallout pattern at an altitude h = 1 meter in r/hr at time t

C = constant, of appropriate units

W = explosive yield, kt

$I(\bar{h})$ = fraction of the total radioactivity settling on the fallout pattern

x = distance from ground zero along the track axis, km.

The function $F(v)$ is related to the function $N(v)$ by the equation

$$F(v) = k_z\ N(v) \tag{14}$$

where $k_z \cong 4.5 \times 10^3$ r/hr/Ci/km^2, and is determined from the known experimental values in equation (13). The variance term is given by

$$\sigma_y(x) = \frac{\bar{p}}{\sqrt{2\pi}\ p(x,o)} \tag{15}$$

where

$p(x,0)$ = dose rate along the track axis

$\bar{p} = \int_{-\infty}^{\infty} p_1(x,y)dy$ = integral of the transverse distribution at distance x.

Figure 12 shows the relationship of $\sigma_y(x)$ with distance from G.Z. The data are described by the equation

$$\sigma_y(x) = \left[\sigma_o^2 + 0.01\ x^2\right]^{\frac{1}{2}} \tag{16}$$

where σ_o^2 is related to the horizontal dimension of the main cloud and defines the transverse distribution near ground zero. For distances where $\sigma_o^2 \ll 0.01x^2$, $\sigma = 0.1x$. Equation (13) can be rewritten:

$$\frac{0.1\sqrt{2\pi}\, p_t(x,o)\,(HV)^2}{kWI(h)} = v^3 F(v) \approx \varphi(v) \tag{17}$$

in which the right side is a function only of v, the fall velocity of the particles. Experimental data for "1003", Sedan, Danny Boy, and Neptune are used to determine the function $\varphi(v)$. If $p_i(x,0)$ is used for each isotope, then the fallout intensity by isotope can be estimated by the appropriate function $\varphi_i(v)$. The data for "1003" indicate a general relation

$$\varphi(v) \cong v^n \tag{18}$$

which can be used to estimate the dose rate along the track axis by the semi-empirical equation

$$p_t(x,o) = \frac{kWI(h)\,(HV)^n}{\sqrt{2\pi}\,(HV)^2 x^n} \tag{19}$$

For $n = 2$, the H + 24 hour dose rate along the track axis is then

$$p_{24hr}(x,o) = \frac{25WI(h)}{x^2} \tag{20}$$

Thus, equation (20) relates the extent of radioactivity contamination along the close-in fallout track axis to the explosive yield and the fractional deposition along the track. For the general time dependence of mixed radionuclides

$$A(t) = A(t=24hr)\,t^{-1.2} \tag{21}$$

the general expression for the dose rate of fission products in the fallout pattern from an excavation nuclear explosion is given by

$$p_t(x,y) = \frac{1.15\times10^3 WI(h)\,t^{-1.2}}{x^2}\, e^{-y^2/0.02x^2} \tag{22}$$

the infinite-time dose from $t = x/V$ is then

$$D(x,y) = \frac{5.75\times10^3 WI(h)\,V^{0.2}}{x^{2.2}}\, e^{-y^2/0.02x^2} \tag{23}$$

A similar calculation is made for the fallout patterns resulting from the detonation of a row charge of nuclear explosives in which N explosives are emplaced in a line of length L. For the wind direction normal to the row, the doses D_N in the separate fallout tracks are given by

$$D_N(x,y) = ND_1(x,o)\sqrt{\frac{\pi}{2}}\,\frac{\sigma_y}{L}\left[\varphi\left(\frac{L-y}{\sigma_y}\right) + \varphi\left(\frac{y}{\sigma_y}\right)\right] \tag{24}$$

where

$$\varphi(z) = \sqrt{\frac{2}{\pi}} \int_0^z e^{-t^2/2} dt \quad = \text{probability integral}$$

D_1 = dose from a single explosion

$\sigma_y^2 = (0.1x)^2$

For a given dose, the maximum dimension of the zone in direction x is reached when y = L/2, the center of the sector,

$$D_N(x,\frac{L}{2}) = ND_1(x,o) \sqrt{\frac{\pi}{2}}\, 2\, \frac{\sigma_y}{L}\, \varphi(\frac{L}{2\sigma_y}) \tag{25}$$

For canal or other earth-moving projects in which the lengths of individual row-charge explosions will be of the order of tens of kilometers, the ratio $L/2\sigma$ will generally be less than unity. For this case, the expansion of the term $\varphi(z)$ is

$$\varphi(z) = \sqrt{\frac{2}{\pi}}\, z \left[1 - \frac{1}{6} z^2 + ... \right] \tag{26}$$

and

$$D_N(x,\frac{L}{2}) = ND_1(x,o) \left[1 - 0.167 (\frac{L}{2\sigma})^2 + ... \right] \tag{27}$$

Thus the maximum dimension of a fallout zone can be determined for a given total dose, e.g., 0.5r, by the equation

$$D_N(x,\frac{L}{2}) \cong ND_1(x,o) \tag{28}$$

with maximum error $\leq$ 17% when $\frac{L}{2\sigma_y} < 1$.

A similar expression has been calculated for those excavations where an exclusion zone is required and population in that zone returns after some fixed period following the explosion. For a maximum infinite-time dose D^* which accumulates at a distance x^*, at another location $x < x^*$ at which the calculated dose accumulates from time t^* + exclusion time T following the detonation, it is shown that

$$x \cong x^* (\frac{t^*}{T})^{0.1} \tag{29}$$

Equation (29) allows the calculation of the zone of temporary exacuation between the distances x and x^*

Further development is given to estimate the extent of long-range fallout to distances of the order of 10,000 km and to fallout levels which do not exceed the average values of background global fallout, 0.2-0.5 mCi/km^2-day. The fraction of total radioactivity from test "1003" in the long-range fallout was 0.65%. The dispersion of the long-range cloud is based on the semiempirical theory of turbulent diffusion for large-scale averaged meteorological conditions along the cloud trajectory. The source concentration C(x,y,z,t,h) is followed from the instantaneous point source concentration C(o,o,h,o,h) where h = height of the stabilized cloud, with the boundary condition

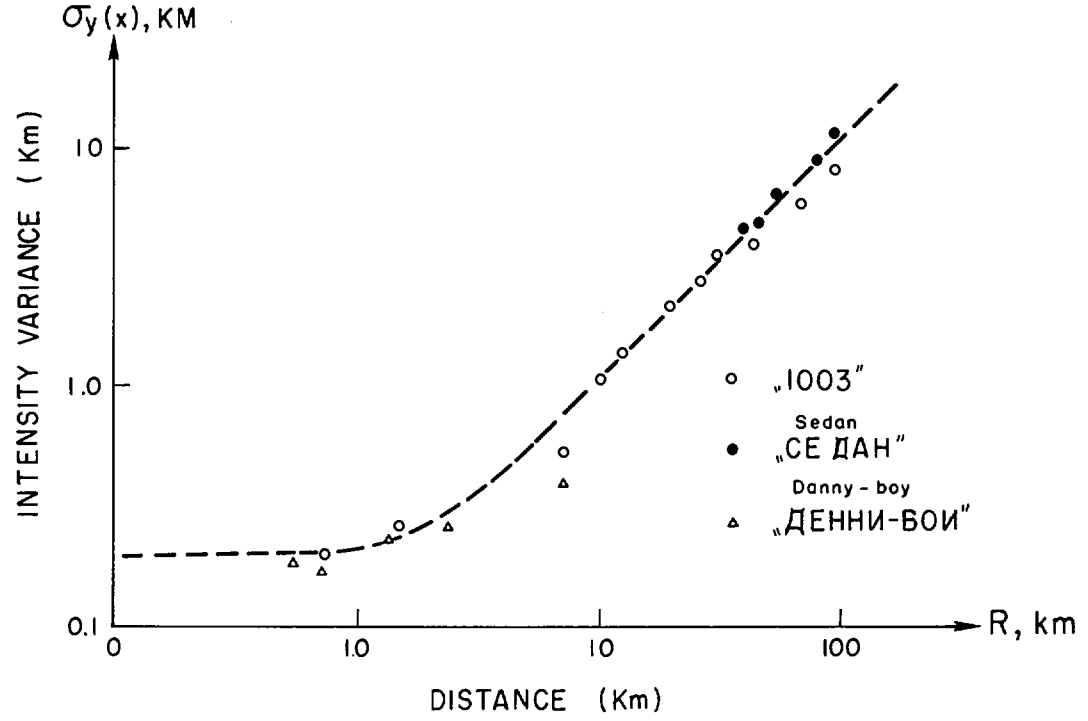

Figure 12. Comparison of the variance of the γ-ray intensity along the track axis of 3 excavation explosions.

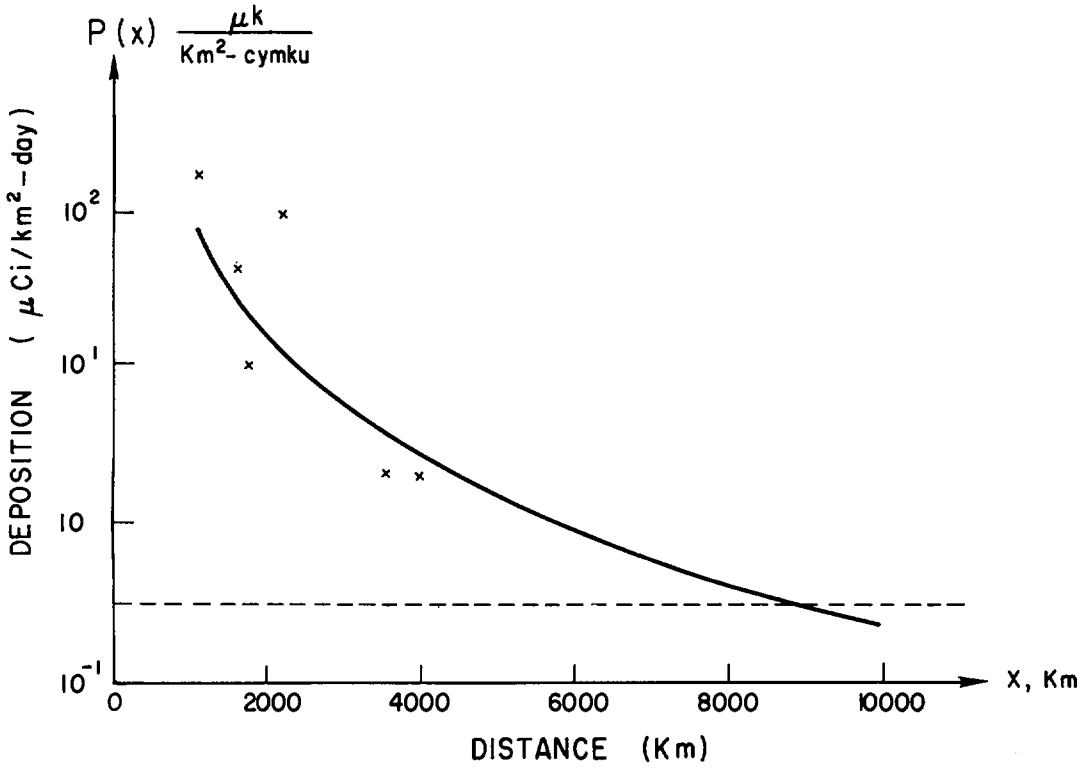

Figure 13. Fallout deposition rate as a function of distance along the track axis.

$$\left(k_z \frac{\partial C}{\partial z} - \beta C\right)_{z=z_o} = 0 \tag{30}$$

where

k_z = vertical diffusion coefficient

β = removal rate constant at the earth's surface (deposition velocity)

The expression for $C(x,y,z,t,h)$ is

$$C = \frac{Q(t)\, e^{-\frac{(x-Vt)^2}{2\sigma_x^2(t)} - \frac{y^2}{2\sigma_y^2(t)}}}{2\pi\, \sigma_x(t)\, \sigma_y(t)} \left[\frac{1}{2\sqrt{\pi k_z t}} \left\{ \exp\left(-\frac{(z-h)^2}{4k_z t}\right) + \exp\left(-\frac{(z+h)^2}{4k_z t}\right) \right\} - \frac{\beta}{k_z} \exp\left(\frac{\beta(z+h)}{k_z} + \frac{\beta^2 t}{k_z}\right) \operatorname{erfc}\left(\frac{\beta\sqrt{t}}{\sqrt{k_z}} + \frac{z+h}{2\sqrt{k_z t}}\right) \right] \tag{31}$$

where $Q(t)$ = total source in the distant fallout. It is assumed that for $t > 2$ days, the dispersion $\sigma(t)$ is given by

$$\sigma(t) \sim \sqrt{t} \tag{32}$$

and for literature values of $k_x = k_y = 10^9$ cm^2/sec and $k_z = 2 \times 10^5$ cm^2/sec,

$$C(x,o,o,t,h) \cong \frac{2.4\times10^{-13}\, h\, Q(t)}{\beta t^{5/2}}\, e^{-\frac{h}{0.3\,t} - \frac{(x-Vt)^2}{1.4\times10^3\, t}} \tag{33}$$

where C is in Ci/m^3. The fallout rate (in Ci/km^2-hr) is then estimated from

$$\Pi = \beta C \tag{34}$$

Figure 13 shows the global fallout deposition rate for the test "1003" using a deposition velocity of $\beta \cong 3.6 \times 10^{-2}$ km/hr.

Acknowledgement

The assistance of the USAEC Division of Peaceful Nuclear Explosives in providing copies of the translations of the two USSR reports is gratefully acknowledged.

REFERENCES

(1) "Mechanical Effect of Underground Nuclear Explosions", Report of the Institute of Terrestrial Physics, USSR Academy of Sciences, Moscow, USSR, 1969.

(2) U. A. Izrael, V. N. Petrov, A. A. Pressman, F. A. Rovinsky, E. D. Stukin, and A. A. Ter-Saakov, "Radioactive Contamination of the Environment by Underground Nuclear Explosions, and Methods of Forecasting It", Moscow, USSR, 1969.